PHYSICAL REVIEW B **88**, 245302 (2013)

Heteroepitaxy and ferromagnetism of EuO/MgO (001): A route towards combined spin- and symmetry-filter tunneling

Christian Caspers,[1] Andrei Gloskovskij,[2] Wolfgang Drube,[2] Claus M. Schneider,[1,3] and Martina Müller[1,3,*]
[1]*Peter Grünberg Institut (PGI-6) and JARA Jülich-Aachen Research Alliance, Forschungszentrum Jülich, 52425 Jülich, Germany*
[2]*DESY Photon Science, Deutsches Elektronen-Synchrotron, 22607 Hamburg, Germany*
[3]*Fakultät für Physik and Center for Nanointegration Duisburg-Essen (CeNIDE), 47048 Duisburg, Germany*

(Received 8 August 2013; revised manuscript received 25 September 2013; published 5 December 2013)

We demonstrate the high-quality heteroepitaxy of ultrathin EuO films with bulklike ferromagnetism directly on MgO (001), an important step towards combining the spin-filter tunnel effect in magnetic insulators and symmetry-filter tunneling through single-crystalline MgO barriers. Despite a large compressive lattice mismatch, EuO grows fully relaxed on MgO (001) and adopts its bulk lattice parameter from the first monolayer on. This initial heteroepitaxial growth mode is discussed in terms of different electrostatic atomic configurations of the oxides interface. Single-crystalline EuO/MgO (001) thus can be envisioned as highly effective double spin-selective tunnel barriers for spintronics applications.

DOI: 10.1103/PhysRevB.88.245302 PACS number(s): 75.47.Lx, 85.75.−d, 77.55.Px, 73.40.Qv

I. INTRODUCTION

Functional oxides are at the heart of future spin electronics, as they allow one to couple various ferroic order parameters and conductivities into multifunctional heterostructures. In particular, the magnetic oxide EuO unites the rare combination of ferromagnetic order ($T_C = 69.3$ K) and insulating properties.[1] With its exchange-split conduction band of 0.6 eV,[2] ultrathin EuO enables efficient spin filtering via different tunnel barrier heights for majority and minority electrons.[3] In single-crystalline bcc ferromagnet/MgO-based tunnel junctions, spin selection is due to the well-studied $\Delta_{1,5}$ symmetry-filter effect.[4,5] Combining both spin- and symmetry-filtering in a double-tunnel barrier may result in truly 100% spin-polarized tunnel currents and significant tunnel magnetoresistance (TMR) ratios, both directly relying on the two most efficient spin-dependent tunneling mechanisms in functional oxide materials.[6–8]

A precondition to establishing symmetry-dependent spin tunneling is the high-quality heteroepitaxy of EuO/MgO (001) and its interface, which enables the coherent tunnel transport of evanescent electronic states. Symmetry-dependent tunneling through either single-crystalline EuO or MgO barriers has been elucidated in complex band structure models.[9–11] Under certain conditions, both EuO (001) and MgO (001) barriers may provide significant tunneling spin selectivity via free-electron bands of Δ_1 symmetry; however, no theoretical description of the combined spin- and symmetry-dependent tunnel transport through this ferromagnetic/nonmagnetic double barrier exists to date.

On the experimental side, Miao and Moodera[12] have recently observed TMR in an EuO/MgO-based magnetic tunnel junction. In this study, polycrystalline EuO composed of both oxygen-rich and stoichiometric phases was utilized, thus hampering single crystallinity of the magnetic tunnel barrier and the EuO/MgO transport interface, leading to moderate TMR ratios only. The major experimental difficulty relies in synthesizing the metastable oxide EuO in its stoichiometric ferromagnetic phase since off-stoichiometry precludes an epitaxial growth and also reduces ferromagnetic exchange in the ultrathin-film limit, which is, however, essential for efficient spin-filter tunneling.[13–17]

In recent years, several growth studies on EuO thin films have been presented, in particular on stoichiometric EuO thin films grown coherently on perfectly lattice-matched yttria-stabilized zirconia (YSZ)[14,18] and on different cubic oxides with only a few percent tensile lattice strain.[19,20] The system EuO/MgO (001), however, provides a large compressive lattice mismatch of $m = (a_{\mathrm{MgO}} - a_{\mathrm{EuO}})/a_{\mathrm{EuO}} = -18\%$. A few works already report heteroepitaxy and bulklike magnetization of EuO on MgO, but with EuO film thicknesses above several tens of nanometers.[18,21] A recent study by Swartz *et al.*[20] concludes that ultrathin EuO heteroepitaxy on MgO (001) cannot be obtained with film thicknesses below 2 nm. That study also reports the formation of polycrystalline EuO in the initial monolayer regime without any additional oxygen supply. EuO/MgO (001) heteroepitaxy was only realized by the insertion of a TiO_2 buffer layer.[20]

In this study, we demonstrate the high-quality heteroepitaxy of EuO ultrathin films directly on MgO (001) from the initial monolayer on. The bulklike ferromagnetic properties of ultrathin EuO/MgO (001) clearly indicate a fully relaxed oxide heteroepitaxy and coincide very well with an *in situ* structural surface analysis. Consequently, an atomically sharp, crystalline EuO/MgO (001) transport interface is established, as verified by *ex situ* electron and x-ray diffraction experiments. A chemical study employing hard x-ray photoelectron spectroscopy (HAXPES) reveals the ideal EuO stoichiometry. Based on these complementing experimental results, we propose possible electrostatic atomic configurations of the EuO/MgO (001) oxide heterointerface and discuss their validity in the context of magnetostatic simulations. Our results may serve as important input for future experimental works as well as for theoretical modeling of electronic structure-dependent transport mechanisms.

II. EXPERIMENTAL DETAILS

Ultrathin EuO films were synthesized on MgO (001) substrates by reactive molecular beam epitaxy (MBE) under

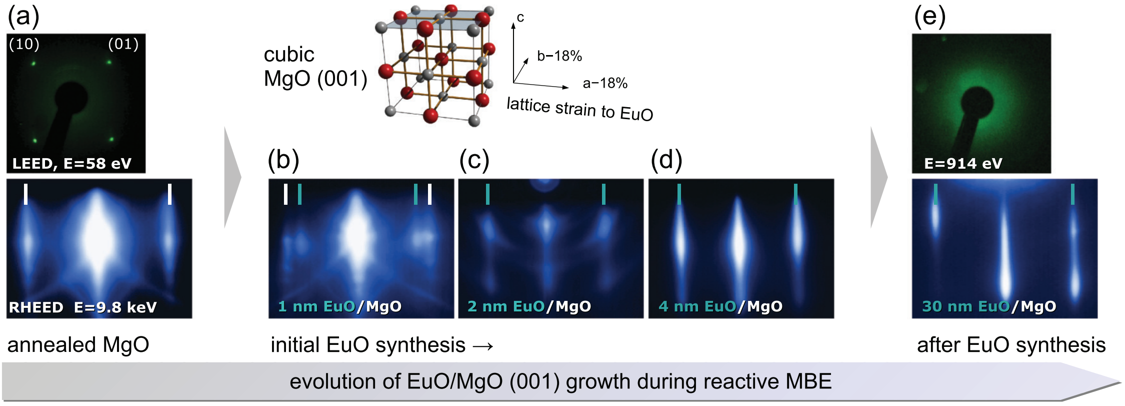

FIG. 1. (Color online) Evolution of the surface crystal structure during EuO growth directly on MgO (001). The RHEED pattern along the [010] direction confirms EuO/MgO heteroepitaxy. After growth, EuO film roughness hampers the observation of LEED pattern.

UHV conditions ($p_{\text{base}} \leqslant 5 \times 10^{-11}$ mbar). The MgO substrates were annealed at $T_S = 650\,^{\circ}$C under a molecular oxygen supply of $p_{\text{ox}} = 10^{-7}$ mbar for several hours.

In order to synthesize stoichiometric EuO, we apply the Eu distillation condition,[2,18] i.e., evaporating excess Eu metal (99.99%) at elevated substrate temperature in a limited oxygen supply. First, we deposit an Eu metal seed layer in the monolayer regime just before EuO synthesis in order to account for the additional oxygen supply from the MgO substrate. Second, in order to start the EuO formation on the Eu-covered MgO substrate, we manually ramp up the molecular oxygen for the EuO oxidation reaction. This, in particular, is only possible using a differentially pumped gas supply and gas nozzles with a fine-adjusted sample distance. The subsequent EuO adsorption is then controlled by a meticulous regulation of the oxygen supply in the 10^{-9} mbar regime. Due to their metastable character, the ultrathin EuO films are finally capped with 5-nm Si, and high vacuum storage conditions are persistently maintained.

We perform structural investigations of the EuO/MgO (001) heterostructures by employing *in situ* reflection high-energy electron diffraction (RHEED), low-energy electron diffraction (LEED), and *ex situ* x-ray diffraction (XRD). Magnetization measurements were carried out using a Quantum Design MPMS XL superconducting quantum interference device (SQUID) magnetometer. HAXPES experiments were conducted at beam line P09 at PETRA III (DESY, Hamburg).

III. RESULTS

A. Oxide heteroepitaxy and structural properties

We investigate the growth of EuO directly on MgO (001) by monitoring the surface crystalline structure via *in situ* electron diffraction techniques. In Fig. 1(a), the annealed MgO substrate shows sharp RHEED and LEED patterns, indicating a single-crystalline and smooth surface. For the first one to two monolayers of EuO growth in Fig. 1(b), we observe streaky RHEED patterns of MgO and EuO simultaneously. We find the EuO cubic RHEED pattern to be apparent at any time of growth. This result clearly demonstrates the heteroepitaxy of EuO on MgO (001), with no polycrystalline interface phase within the detection limit. A quantitative analysis of the RHEED pattern of the first monolayer EuO yields a lattice parameter of $a_{\parallel} = 5.14 \pm 0.11$ Å, which equals the lattice parameter of the EuO cubic cell, $a = 5.142$ Å. This observation suggests that unstrained EuO has formed directly on MgO (001). During further EuO synthesis, i.e., from the second EuO nanometer on, weak circular RHEED intensities occur in addition to the dominating stripe pattern of unstrained EuO in Fig. 1(c). Thus, a small fraction of dislocations has formed once the EuO layer is closed. Until the end of EuO deposition, the surface crystal structure of EuO improves, and heteroepitaxy is maintained. Indeed, for EuO thicknesses above 4 nm the RHEED patterns in Fig. 1(d) indicate a smooth and highly crystalline EuO surface, similar to the results of single-crystalline EuO grown on lattice-matched YSZ (001).[22] After sustained growth of 30-nm EuO/MgO (001), the roughening of the initial EuO layers hampers us from observing an fcc structure within the LEED beam coherence length ($\leqslant$100 Å). Due to its larger spatial average and smaller coherent length, however, a clear cubic structure is observable by RHEED in Fig. 1(e).

Moving on to the investigation of the bulk crystal structure and interface properties of EuO/MgO (001) heterostructures, we performed *ex situ* high-resolution x-ray diffraction scans. In Fig. 2(a), we show the measured x-ray reflectivity data and the simulated Kiessig fringes by a Parratt model. In this way, we deduce the thickness of the EuO layer ($d_{\text{EuO}} = 4$ nm) and its roughness ($\sigma_{\text{EuO}} = 0.8$ nm). Consistent with the *in situ* RHEED experiments, we confirm the experimental lattice parameter of EuO equals the literature value of bulk EuO. We exclusively observe diffraction peaks of the EuO ($h\,0\,0$) cubic planes from a wide 2θ-θ survey in Fig. 2(b). The occurrence of Kiessig fringes around the EuO diffraction peaks indicates smooth interfaces of the ultrathin EuO slab. The high crystal quality of the EuO film is confirmed by the FWHM of the EuO (200) rocking curve, which amounts to 0.025° and thus is comparable to the FWHM of the underlying MgO (200) rocking curve [see inset in Fig. 2(b)]. We note in parenthesis that a determination of the initial EuO in-plane lattice parameter by XRD is not feasible since the peak broadening due to a finite roughness of the subsequent EuO film would overlay any strain information of the initial EuO layer.

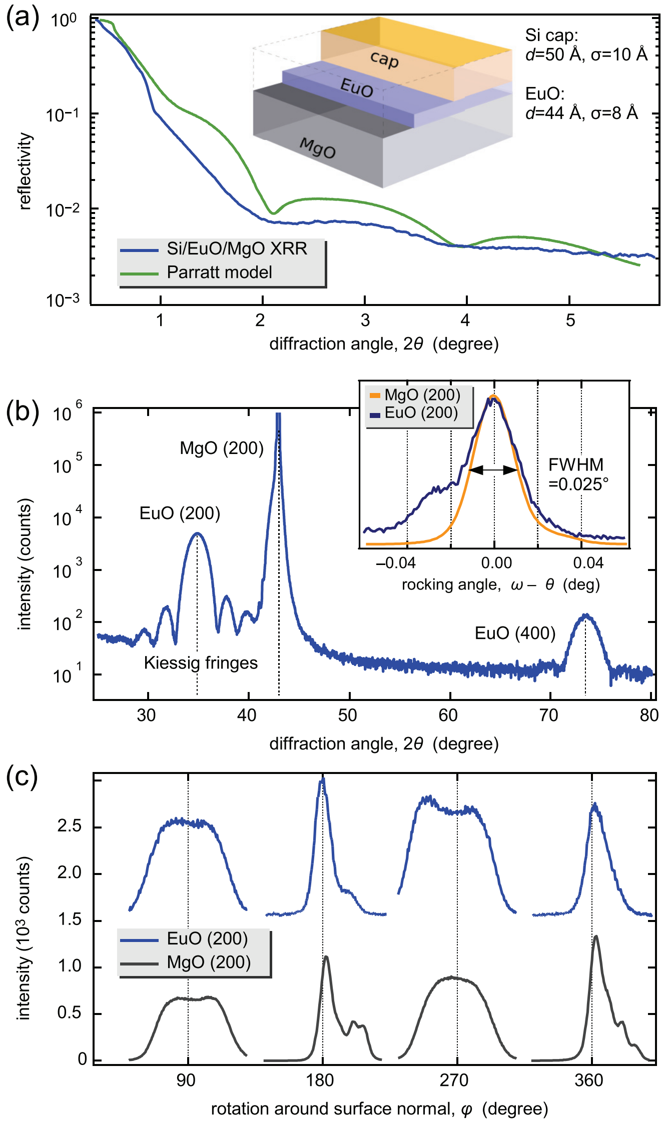

FIG. 2. (Color online) X-ray diffraction of Si/(4 nm)EuO/MgO (001). (a) Parratt fitting reveals the thickness and roughness of EuO. (b) A 2θ wide scan shows Bragg reflections of the MgO substrate and the EuO ultrathin film. The inset shows the rocking curve of the EuO (200) reflex. (c) The epitaxial relationship between EuO/MgO (001) is confirmed by a ϕ scan.

We provide further evidence for the epitaxial relation between MgO (001) and the ultrathin EuO film with a full rotational diffraction scan around the surface normal (ϕ scan) in Fig. 2(c). The ϕ scan shows the same fourfold symmetry for the MgO (200) as for the EuO (200) diffraction peak. Obviously, the broadening at the positions $\phi = 90^\circ$ and 270° originates from a faceting of the MgO substrate, which is adopted by the EuO crystalline film.

B. Electronic properties

In order to investigate the chemical quality and to quantify the stoichiometric composition of the ultrathin EuO films on MgO (001), we conducted a depth-sensitive HAXPES experiment. Figure 3 depicts the Eu $4d$ and $3d_{3/2}$ core-level spectra recorded at a photon energy of $h\nu = 6$ keV and $T = 33$ K. Both spectra show well-resolved final-state multiplets, which agree very well with photoemission multiplets of Eu^{2+} ions from experimental studies of divalent Eu compounds[15,16] and theoretical multiplet calculations.[23,24] At the high-binding-energy side, smaller spectral contributions are observable, which are part of the complex Eu^{2+} final-state multiplet and do not indicate any different EuO phases, e.g., Eu^{3+} ions.

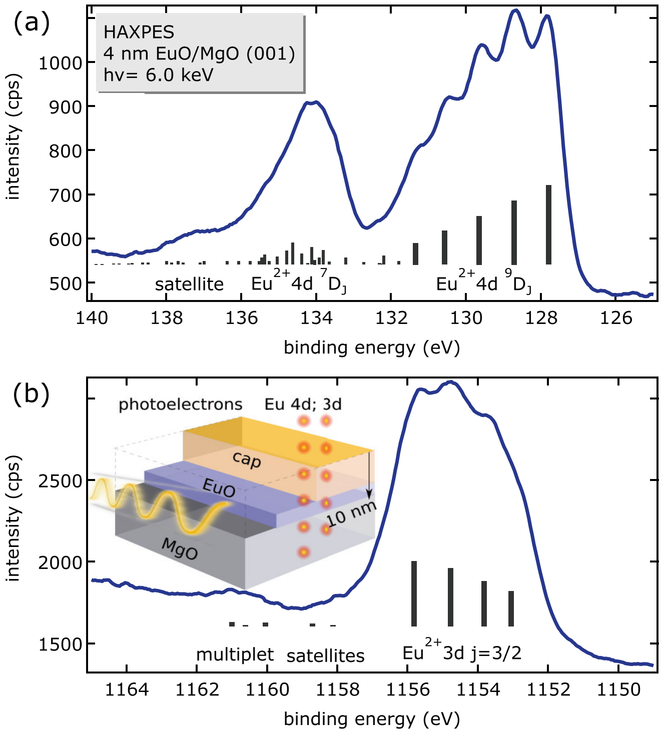

FIG. 3. (Color online) HAXPES of a Si/(4 nm)EuO/MgO heterostructure. (a) Eu $3d$ and (b) Eu $4d$ core level spectra recorded at 6 keV and 33 K. Both well-resolved multiplets reveal a Eu^{2+} valency, indicative of stoichiometric and ferromagnetic EuO.

In conclusion, the EuO/MgO heterostructures show a fully 2+ valency, as expected for the purely divalent and stoichiometric EuO, and no indications of metallic phases or higher oxides.

C. Magnetic properties

Next, we characterize the magnetic properties of 4- and 30-nm-thick heteroepitaxial EuO/MgO (001) samples by SQUID magnetometry, measured in plane along the cubic [010] direction in an aligning field $H = 10$ Oe. The results are compared to two single-crystalline and fully lattice-matched EuO/YSZ (001)[22] reference systems in Fig. 4.

A bulk EuO/MgO (001) sample with $d_{\mathrm{EuO}} = 30$ nm shows a Curie temperature of $T_C = 69$ K, which perfectly matches that of a 30-nm-thick EuO reference sample on a lattice-matched YSZ (001) substrate. The magnetization curve thereby follows a Brillouin function with $S = 7/2$. Moving on to the $M(T)$ characteristics of an ultrathin EuO film ($d_{\mathrm{EuO}} = 4$ nm) on MgO (001), we find the $M(T)$ curve deviating less than 5% from the 30-nm-thick EuO/MgO (001) film. The Curie temperature of the ultrathin EuO film is slightly reduced to 67 K, i.e., 2 K below the bulk value. This reduction of T_C is comparable to

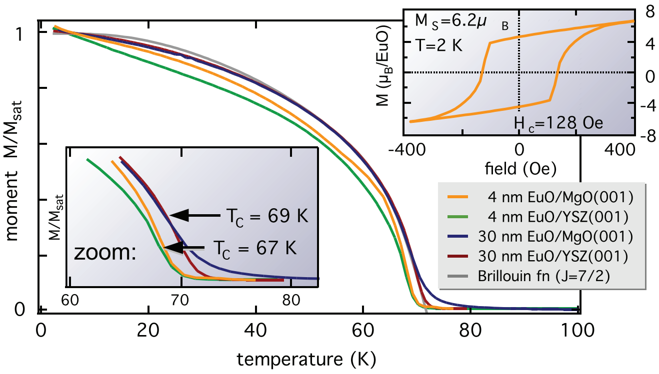

FIG. 4. (Color online) Magnetic properties of heteroepitaxial EuO on MgO (001) and, for reference, on lattice-matched YSZ (001). A Brillouin-shaped $M(T)$ curve with bulklike T_C is observed for EuO film thicknesses of both $d = 4$ and 30 nm. Arrows indicate changes in T_C due to thickness effects.

that of the single-crystalline and lattice-matched 4-nm-thick EuO/YSZ (001) reference sample.[22] Thus, we attribute this small deviation of T_C to the reduced dimensionality of the ultrathin EuO film rather than a strain-induced modification of magnetic exchange interactions.[13,25]

In the inset of Fig. 4, the $M(H)$ hysteresis loop of a 4-nm EuO/MgO (001) encloses a rectangular area with well-defined magnetic switching points. The coercive field of the ultrathin EuO film amounts to $H_c = 128$ Oe and thus is about three times the value of an optimum 4-nm EuO/YSZ (001) heterostructure.[22] This result is a further hint regarding the presence of structural dislocations in the EuO layers on MgO (001), as already indicated by RHEED. These crystalline defects probably give rise to a pinning of magnetic domains in EuO and thus increase the coercive field. We note that the observed coercive field is significantly smaller than that of a similar EuO heterostructure grown by Swartz *et al.*,[20] who inserted an TiO_2 buffer on the MgO (001) substrate in order to circumvent the large lattice mismatch. The observed bulklike magnetic properties underline the high epitaxial quality of even ultrathin EuO films on MgO (001). The sizable increase of the EuO coercive field suggests the formation of structural domains, as will be discussed in more detail in the following.

IV. DISCUSSION

From the structural and magnetic investigations we conclude that the EuO ultrathin films grow heteroepitaxially but fully unstrained on MgO (001) substrates, despite a large compressive lattice mismatch of $m = -18\%$. In order to further elucidate this heteroepitaxial growth mode, we discuss the initial stages of the EuO thin-film growth with regard to its fracture mechanics and discuss possible atomic configurations of the EuO:MgO interface with respect to the electrostatic properties.

The EuO lattice relaxation on a biaxially compressive substrate may introduce misfit dislocations in the form of vertical cracks. Whereas in metals ductile elasticity allows for relatively large lattice strains before fracture occurs, the critical strain $\varepsilon_{\text{crit}}$ at which cracks in thin oxide layers are predicted is typically smaller and is given by[26–28]

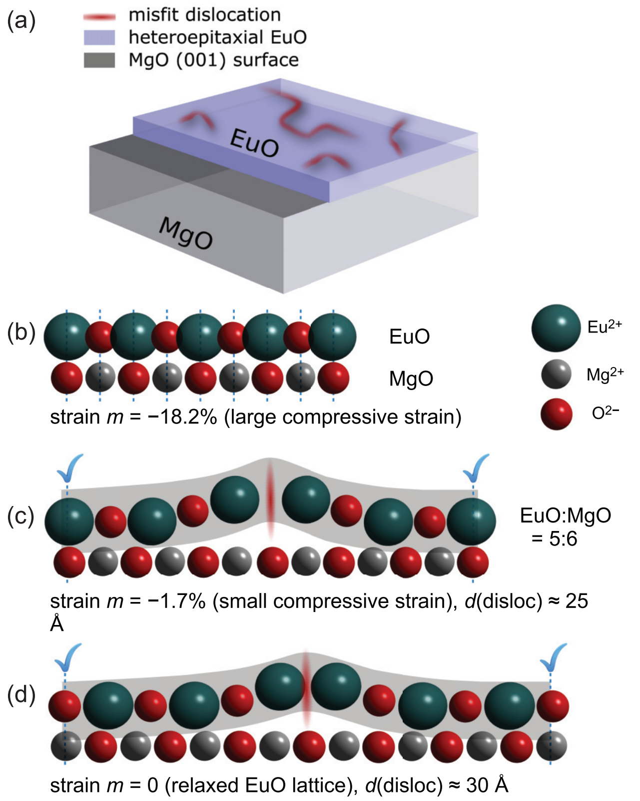

FIG. 5. (Color online) Heteroepitaxial configurations of the EuO/MgO (001) interface. (a) Schematics of the EuO/MgO (001) heterosystem with structural misfit dislocations. (b) A cube-on-cube relation induces large compressive strain to EuO. In the EuO/MgO 5:6 configuration (c), a small compressive strain of −1.7% acts on EuO. (d) If EuO grows fully relaxed on MgO (001), electrostatic repulsion leads to structural misfit dislocations at larger distances.

$$\varepsilon_{\text{crit}} > \left(\frac{2}{d}\frac{\gamma}{E}\right)^{\frac{1}{2}}. \tag{1}$$

Here, γ denotes the surface fracture energy, d is the thickness of the oxide overlayer, and E is Young's modulus of the oxide. We evaluate Eq. (1) with empirical values of oxides[28] and a film thickness of $d_{\text{EuO}} = 4$ nm. This yields a critical strain of $\varepsilon_{\text{crit}} \approx 6\%$, above which cracks in the EuO overlayer should be expected.

This finding suggests the formation of misfit dislocations in EuO [Fig. 5(a)] because the film-substrate lattice misfit needs to be compensated at particular positions, as is evidenced by our structural and magnetic results.

In order to understand the occurrence of structural dislocations in EuO/MgO (001) on a microscopic basis, we consider the electrostatic properties at the heterointerface. As illustrated in Fig. 5, the significantly different ionic radii of Eu^{2+}, O^{2-}, and Mg^{2+} ions give rise to strong Coulomb repulsion dependent on their atomic configuration at the EuO:MgO interface. Consequently, the ionic arrangement determines the EuO morphology and formation of structural dislocations, as will be discussed in the following.

An intuitive scenario is the direct cube-on-cube heteroepitaxy, which adopts the lateral compressive strain of

$m = -18\%$ provided by the MgO substrate [Fig. 5(b)]. Due to electrostatic Coulomb repulsion, however, the large ionic diameter of the Eu^{2+} ions (2.48 Å)[29] would force either the Eu^{2+} or the O^{2-} ions to find equilibrium positions in the vertical direction.[20] This configuration would lead to a strongly roughened surface and destroy heteroepitaxy already from the first EuO monolayers on. From Eq. (1) and our RHEED investigation (Fig. 1), we can exclude a direct cube-on-cube heteroepitaxy.

Next, we consider a lateral arrangement of EuO/MgO = 5:6, as sketched in Fig. 5(c). This configuration would provide a significantly reduced compressive strain of $m = -1.7\%$ and thus would lie well below the critical limit for fracture strain according to Eq. (1). In this 5:6 configuration, strong Coulomb repulsion between O^{2-}-O^{2-} and Eu^{2+}-Mg^{2+} ions, as indicated by red dislocations symbols in Fig. 5(c), also leads to structural roughening at the interface due to misfit dislocations. We estimate the average distance between misfit dislocations in this model as ∼25 Å. With regard to the magnetic properties, the small lattice compression would lead to a sizable increase of the EuO magnetic exchange, which in turn would enhance the Curie temperature by about 8 K.[25] This effect, however, is not observed in our $M(T)$ experiments.

Another possible heteroepitaxial configuration of EuO/MgO = 4:5 provides a small tensile strain of EuO, $m = +2.4\%$ (not shown in Fig. 5).[20] This tensile strain is predicted to strongly decrease the Curie temperature of the ultrathin EuO film by about 14 K.[25] Such a sizable effect is not observed in our magnetic characterization (Fig. 4), and thus, we can exclude this atomic arrangement.

We instead propose an alternative electrostatic configuration, which comprises a fully laterally relaxed EuO ultrathin film on MgO (001). This configuration is supported by our magnetic measurements, which reveal nearly identical magnetization vs temperature curves of heteroepitaxial EuO/MgO (001) and lattice-matched EuO/YSZ (001), as well as by electron diffraction studies of bulklike EuO/MgO (001).[18] Here, no simple integer relation of EuO:MgO cubic cells can be outlined. In this arrangement, the smaller lattice constant of the MgO (001) substrate does not compress the EuO crystal, but misfit dislocations relax the EuO overlayer within the first one or two monolayers [Fig. 5(d)]. We estimate that regions of heteroepitaxy are maintained over a larger region with an average periodicity of more than ∼30 Å. The RHEED pattern and the magnetization curves of EuO/MgO (001) are almost identical to lattice-matched EuO/YSZ (001), which is fully consistent with the model of a fully relaxed EuO/MgO (001) interface configuration.

From the presented structural, electronic, and magnetic results, we conclude that the construction of epitaxial EuO/MgO-based hybrid tunnel junctions with bulklike ferromagnetic properties should be feasible. We consider a nearly perfect oxide stoichiometry as an important prerequisite for an optimum electrical tunnel barrier performance. Oxygen defects, either in the EuO barrier or in the MgO barrier, would open up additional electron conduction channels and lead to an unwanted metallic conductivity. Furthermore, both the presence of oxygen defects or the overoxidation towards Eu^{3+} would be detrimental for spin-filter tunneling, as they cause spin scattering at unordered magnetic defect levels or electron scattering at nonmagnetic Eu^{3+}, respectively. Finally, an atomically sharp and heteroepitaxial EuO:MgO transport interface is important to coherently couple the evanescent electronic states between the two barriers. In particular, the finding of a fully relaxed EuO/MgO (001) interface suggests that bulklike electronic properties and band structure lead to the maximal efficiency of the oxide heterostructure. This finding furthermore allows the realistic *ab initio* modeling of the band-structure-dependent electrical transport, which would give further fundamental insights into this efficient, but complex, spin-dependent tunneling mechanism.

V. SUMMARY

In summary, we presented a detailed growth study and magnetic analysis of ultrathin EuO/MgO (001), a model system for combining spin-filter- and symmetry-dependent tunneling into a double-functional tunnel barrier. We established the heteroepitaxy of ultrathin EuO directly on MgO (001), despite a large compressive lattice mismatch. Surprisingly, we find the EuO ultrathin films growing fully relaxed with its native lattice constant from the first monolayer on. This finding agrees with the finding of a bulklike magnetization for ultrathin EuO/MgO (001) and is discussed in the frame of possible electrostatic atomic configurations of the EuO/MgO (001) interface. We consider this result highly relevant for a theoretical modeling of the tunnel transport in EuO/MgO (001), which may combine the two most effective spin-selective tunneling mechanisms. Given the above findings, the EuO/MgO (001) system is envisioned as a highly efficient double spin-selective tunnel barrier for future oxide spintronics applications.

ACKNOWLEDGMENTS

We acknowledge experimental support during beam times by B. Zijlstra and M. Hoppe. The HAXPES instrument at beam line P09 is jointly operated by the University of Würzburg (R. Claessen), the University of Mainz (C. Felser), and DESY. Funding by the Federal Ministry of Education and Research (BMBF) under Contracts No. 05KS7UM1, No. 05K10UMA, No. 05KS7WW3, and No. 05K10WW1 is gratefully acknowledged. M.M. acknowledges financial support by DFG under Grant No. MU3160/1-1 and by HGF under Contract No. VH-NG-811.

---

[*] mart.mueller@fz-juelich.de

[1] A. Mauger and C. Godart, Phys. Rep. **141**, 51 (1986).

[2] P. G. Steeneken, L. H. Tjeng, I. Elfimov, G. A. Sawatzky, G. Ghiringhelli, N. B. Brookes, and D.-J. Huang, Phys. Rev. Lett. **88**, 047201 (2002).

[3] T. S. Santos and J. S. Moodera, Phys. Rev. B **69**, 241203 (2004).

[4] S. Yuasa, T. Nagahama, A. Fukushima, Y. Suzuki, and K. Ando, Nat. Mat. **3**, 868 (2004).

[5] S. S. P. Parkin, C. Kaiser, A. Panchula, P. M. Rice, B. Hughes, M. Samant, and S.-H. Yang, Nat. Mater. **3**, 862 (2004).

[6] G.-X. Miao, M. Münzenberg, and J. S. Moodera, Rep. Prog. Phys. **74**, 036501 (2011).

[7] M. Müller, G.-X. Miao, and J. S. Moodera, Europhys. Lett. **88**, 47006 (2009).

[8] G.-X. Miao, M. Müller, and J. S. Moodera, Phys. Rev. Lett. **102**, 076601 (2009).

[9] P. V. Lukashev, A. L. Wysocki, J. P. Velev, M. van Schilfgaarde, S. S. Jaswal, K. D. Belashchenko, and E. Y. Tsymbal, Phys. Rev. B **85**, 224414 (2012).

[10] N. Jutong, I. Rungger, C. Schuster, U. Eckern, S. Sanvito, and U. Schwingenschlögl, Phys. Rev. B **86**, 205310 (2012).

[11] W. H. Butler, Sci. Technol. Adv. Mater. **9**, 014106 (2008).

[12] G.-X. Miao and J. S. Moodera, Phys. Rev. B **85**, 144424 (2012).

[13] M. Müller, G.-X. Miao, and J. S. Moodera, J. Appl. Phys. **105**, 07C917 (2009).

[14] S. G. Altendorf, A. Efimenko, V. Oliana, H. Kierspel, A. D. Rata, and L. H. Tjeng, Phys. Rev. B **84**, 155442 (2011).

[15] C. Caspers, M. Müller, A. X. Gray, A. M. Kaiser, A. Gloskovskii, C. S. Fadley, W. Drube, and C. M. Schneider, Phys. Rev. B **84**, 205217 (2011).

[16] C. Caspers, M. Müller, A. X. Gray, A. M. Kaiser, A. Gloskovskii, C. S. Fadley, W. Drube, and C. M. Schneider, Phys. Status Solidi RRL **5**, 441 (2011).

[17] C. Caspers, S. D. Flade, M. Gorgoi, A. Gloskovskii, W. Drube, C. M. Schneider, and M. Müller, J. Appl. Phys. **113**, 17C505 (2013).

[18] R. Sutarto, S. G. Altendorf, B. Coloru, M. Moretti Sala, T. Haupricht, C. F. Chang, Z. Hu, C. Schüßler-Langeheine, N. Hollmann, H. Kierspel, H. H. Hsieh, H.-J. Lin, C. T. Chen, and L. H. Tjeng, Phys. Rev. B **79**, 205318 (2009).

[19] A. Melville, T. Mairoser, A. Schmehl, T. Birol, T. Heeg, B. Hollander, J. Schubert, C. J. Fennie, and D. G. Schlom, Appl. Phys. Lett. **102**, 062404 (2013).

[20] A. G. Swartz, J. J. I. Wong, I. V. Pinchuk, and R. K. Kawakami, J. Appl. Phys. **111**, 083912 (2012).

[21] N. Iwata, G. Pindoria, T. Morishita, and K. Kohn, J. Phys. Soc. Jpn. **69**, 230 (2000).

[22] C. Caspers, M. Müller *et al.* (unpublished).

[23] E.-J. Cho, S.-J. Oh, S. Imada, S. Suga, T. Suzuki, and T. Kasuya, Phys. Rev. B **51**, 10146 (1995).

[24] C. Gerth, K. Godehusen, M. Richter, P. Zimmermann, J. Schulz, P. Wernet, B. Sonntag, A. G. Kochur, and I. D. Petrov, Phys. Rev. A **61**, 022713 (2000).

[25] N. J. C. Ingle and I. S. Elfimov, Phys. Rev. B **77**, 121202 (2008).

[26] J. Armitt, D. R. Holmes, M. I. Manning, D. B. Meadowcroft, and E. Metcalfe, EPRI Report No. FP-686, 1978.

[27] M. Schütze, P. F. Tortorelli, and I. G. Wright, Oxid. Met. **73**, 389 (2010).

[28] J. Robertson and M. I. Manning, Mat. Sci. Technol. **6**, 81 (1990).

[29] D. A. Atwood, *The Rare Earth Elements: Fundamentals and Applications* (Wiley, Hoboken, NJ, 2013).